

Tables

Table 1
Target Weight Percent % (w.r.t to MTOW)

Component	Percent MTOW [%]
Structures	19.00
Propulsion	11.50
System & Equipment	06.00
Mission Fuel	44.20
Payload	14.30
Tolerance	05.00

Table 2
Error % for DOC vs W Optimization

	M	 Error 	σ	 Error 	M	 \Sigma Error	σ	 \Sigma Error
		%		%		%		%
OC	D	-3.005		3.204		08.645		3.359
	W	-10.615		4.777		15.785		5.783

Table 3
Near Field Target Values

Parameter	Target value
n	1/3 to 1/5
$A_{\text{nose}}/A_{\text{net}}$	$\approx 15\%$
\tilde{w}	$\geq 229 \text{ lb/ft}^{n+1}$
Altitude	$\leq 60,000 \text{ ft}$

Table 4

Design variables and Their Relative Values When Optimized for Minimum Noise, Fuel, and Near-Surface Temperature

Parameter	D_{pv} min	dT_{ns} min	dE_{max} min
BPR_{rel}	1.00	1.23	1.23
TTO_{rel}	1.05	1.05	0.95
OPR	23.0	29.0	24.0
$TR_{TO\ rel}$	0.85	1.00	0.95
M_{∞}	1.80	1.80	1.80
W/S_{rel}	0.95	0.97	1.00
$\Delta R_{rel}\%$	-	-	-
	3.00	8.00	14.0
dE_{max} dB	0.20	0.00	-
			6.20
$D_{pv}\%$	-	-17	-
	29.0		4.00
$dT_{ns}\%$	-	-35	-
	8.00		9.00

Table 5

Supersonic Civil Aircraft Material Selection Guidelines

Component	≤ 2 Mach	2 – 4 Mach
Fuselage	Al: 2090-T651, 7075-T6, 8090-T651	CFRP: PMR-15, PMR-11-55, Or new type 2-mm Al-Zn-Mg-Sc-Zr alloy
Skeleton	Ti-6Al-4V	high perf. Ti alloy
Wings	Commercial grade CFRP	CFRP: PMR-15, PMR-11-55, or Ti alloy
Compressor	Ti alloy	Ti-6Al-2Sn-4Zr-6Mo
Combustor & Turbine TBC	SC alloys, DS blades; P/M IN-792 disc, and others	Ni based SC alloys (TMS-75, Rene'N6, CMSX-lfl), MA superalloys; DS blades; P/M IN-792 disc, or advanced alloys

Table 6

Critical Sections and Their Critical Material Selection parameters

Sections	Most Critical Variables
1(Bulk head)	High stiffness, High strength, Low weight
2(Skeleton)	Excellent corrosion resistance, Excellent machinability, High melting point, Low thermal expansion
3(Skin)	Higher elastic modulus, Higher heat resistance, Higher fatigue resistance, High durability, and High specific weight
4(Wings/ also Nose)	Extreme thermal stability, Excellent specific strength, Resistance to extreme temperature gradient, Excellent corrosion resistance

Table 7

Wing Loading During Different Mission Profile

Mission	WL
Take-	88.173
Landing	61.027
Cruise	71.554
Cruise	63.833
Ceiling	55.605
Descent	49.605

Table 8

Wing Sections and Their Optimal Specifications

Sections	Optimal Specifications
1(LREX)	$C_r = 31.05$ m, Area = 43.349 m ² , $\lambda = 0.7$, $\Lambda = 80^\circ$
2(Delta)	Area = 114.553 m ² , $\lambda = 0.4$, $\Lambda = 60^\circ$
3(Outboard)	Area = 67.097 m ² , $\lambda = 0.4$, $\Lambda = 55^\circ$
Overall	Area = 450 m ² , $\bar{c} = 15.9$ m, AR = 3.62

Table 9
Aerodynamic Performance for the Entire Mission Profile

Take off/ landing	M = 0.3	
	$\alpha = 12^\circ$	
	$C_l=1.062$	
	$C_d=0.121$	
Subsonic Cruise	L/D = 8.787	
	M = 0.95	
	$\alpha = 3^\circ$	
	$C_l=0.380$	
Supersonic Cruise	$C_d = 0.027$	
	L/D = 14.171	
	Cooldown	Cruise
	M = 1.6	M = 1.9
	$\alpha = 3^\circ$	$\alpha = 3^\circ$
	$C_l = 0.110$	$C_l=0.094$
	$C_d = 0.012$	$C_d=0.011$
	L/D = 9.152	L/D = 8.488

Table 10
Averages and Deviations of Different Tail Parameters

	L_{rf}/H_f	L_{rf}/L_f	$\alpha_t(^{\circ})$
Conv	3.44-0.397	0.369-0.049	11.59-2.411
T	3.36-0.379	0.351-0.074	11.52-3.102
	AR_H	λ_H	S_{elv}/S_H
Conv	4.49-0.641	0.384-0.082	0.247-0.037
T	4.56-0.594	0.457-0.129	0.341-0.045

Table 11
System Component and Their Corresponding Response Delay

System Component	Delay (Sec)
Accelerometer	0.005 - 0.01
Yaw Rate Sensor	0.005 - 0.01
Side slip Angle (β) Sensor (1)	0.015 - 0.03
Flight Control Computer (2, 3)	0.012 - 0.03
(Assuming a frame rate of 100/sec) Digital to Analog Converter	0.01
Power Actuators	0.02-0.04

Figures

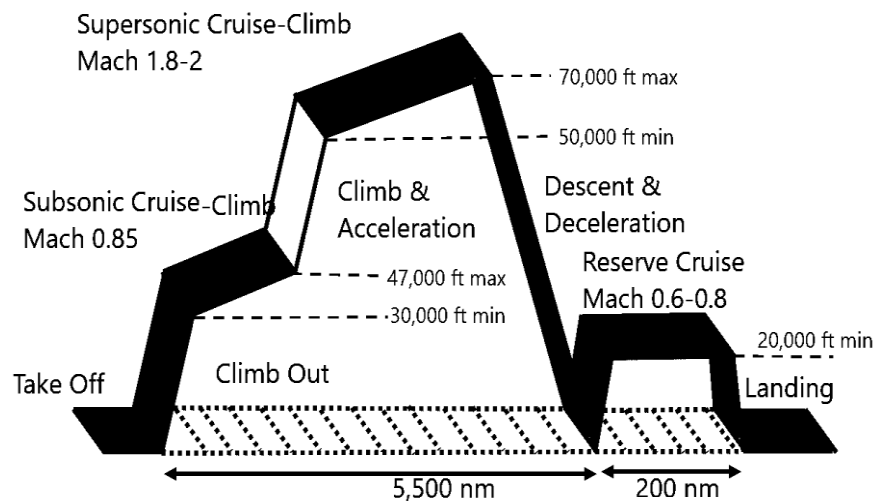


Figure 1: Mission Profile

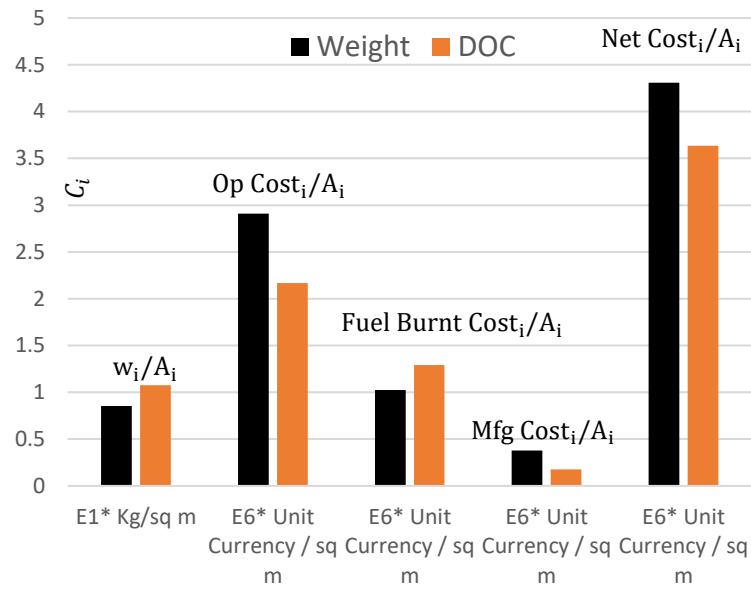


Figure 2: Weight Cost Optimization vs DOC Cost Optimization

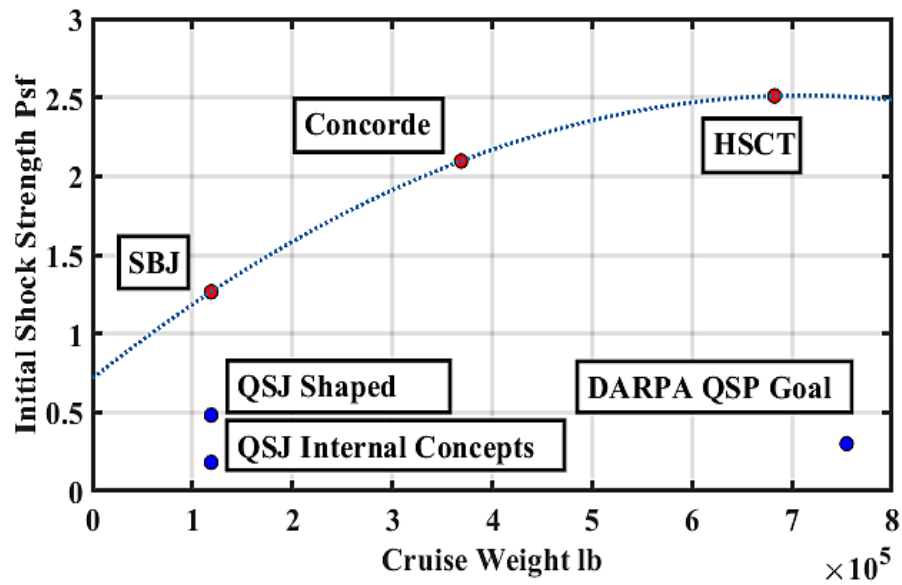


Figure 3: Shock strength of different aircrafts vs their cruise weights

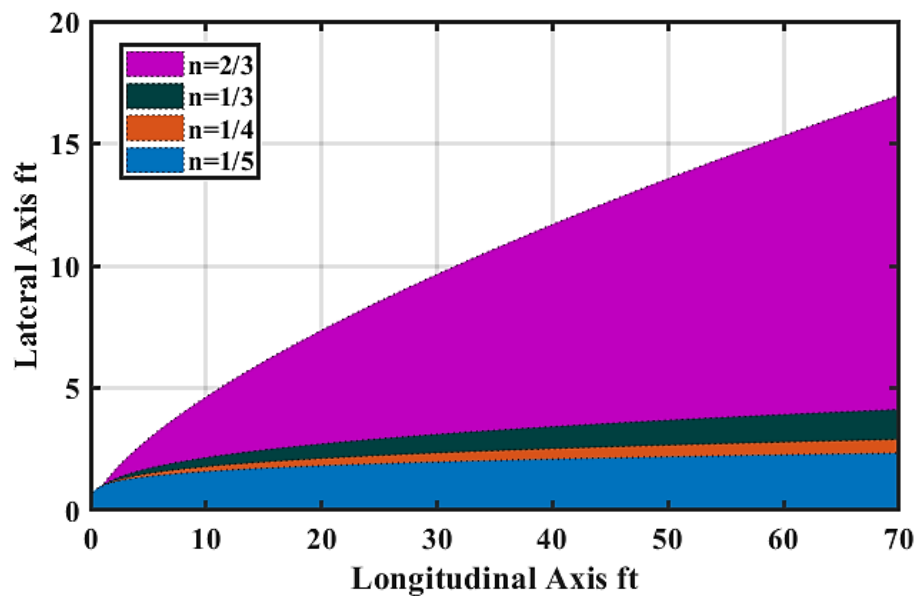


Figure 4: Area Distribution

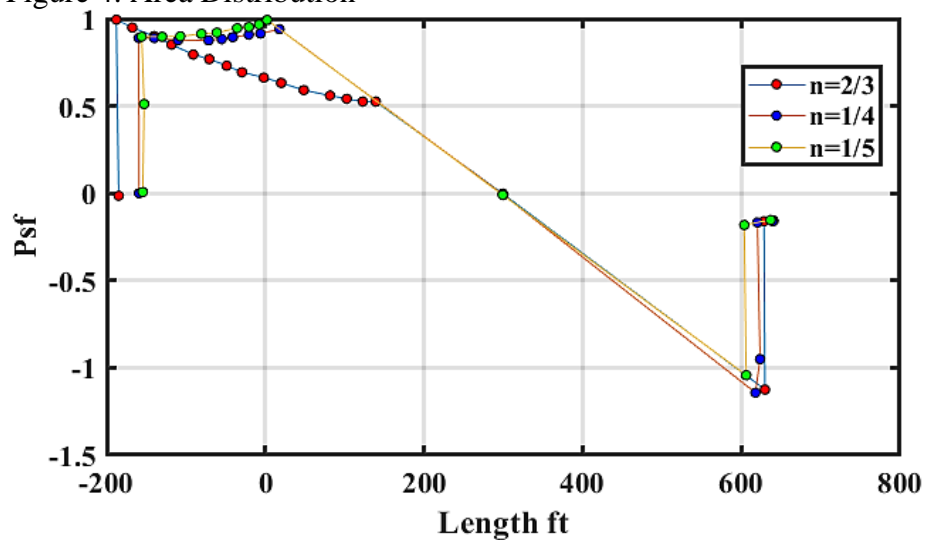


Figure 5: Near-field shock formation for different area distribution

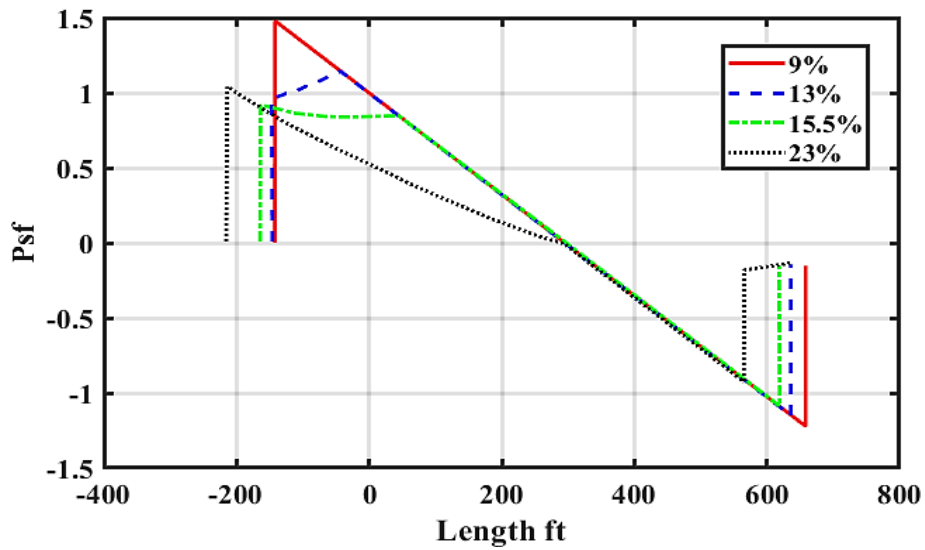


Figure 6: Near field shock formation for different area fraction, where $k=1$ and $n=1/3$

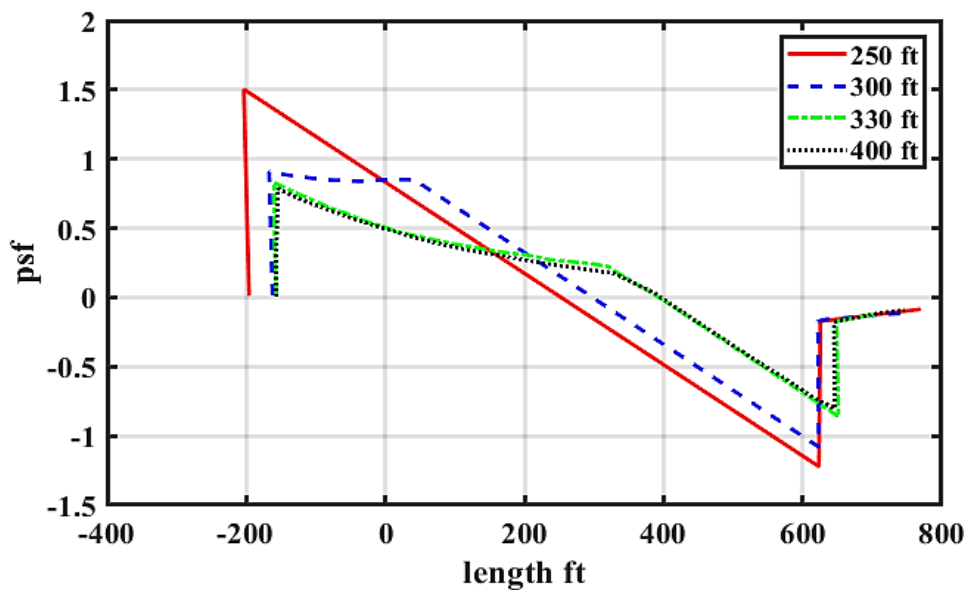


Figure 7: Near Field Shock formation due to different overall length for constant area where $k=1$ and $n=1/3$

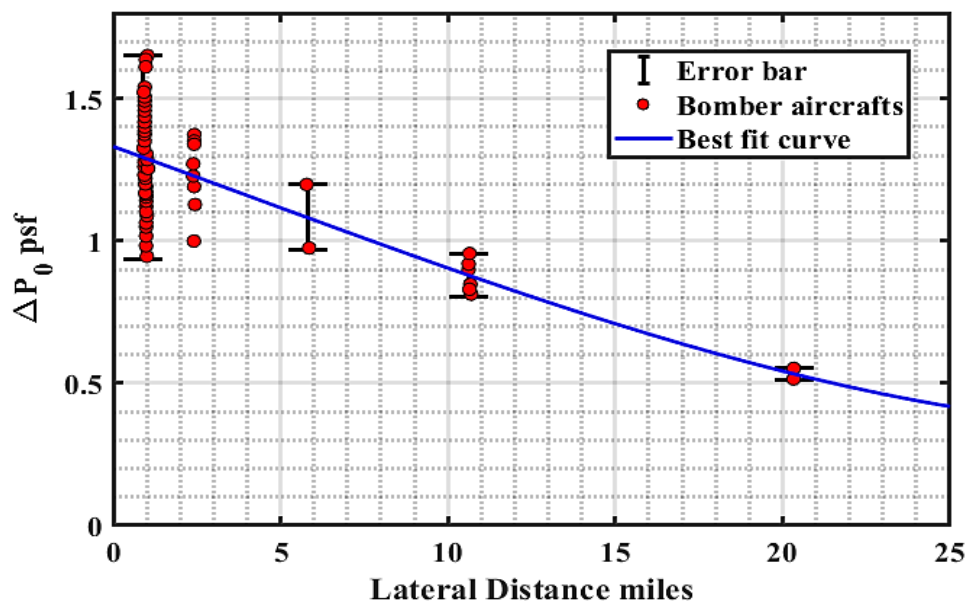


Figure 8: Ground measured shockwave peak overpressure due to high altitude steady flight supersonic bomber aircrafts

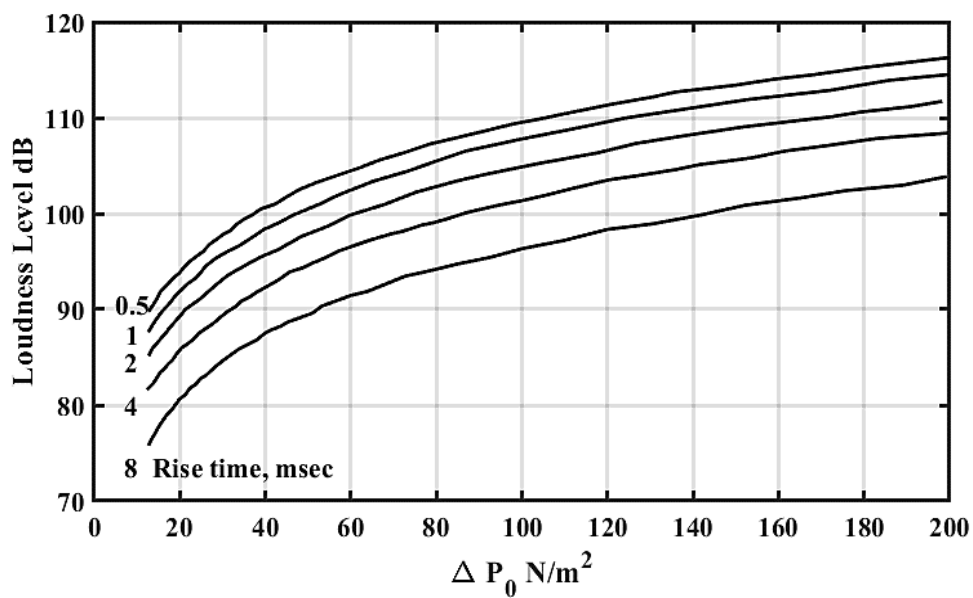


Figure 9: Outdoor ground loudness for different sonic booms

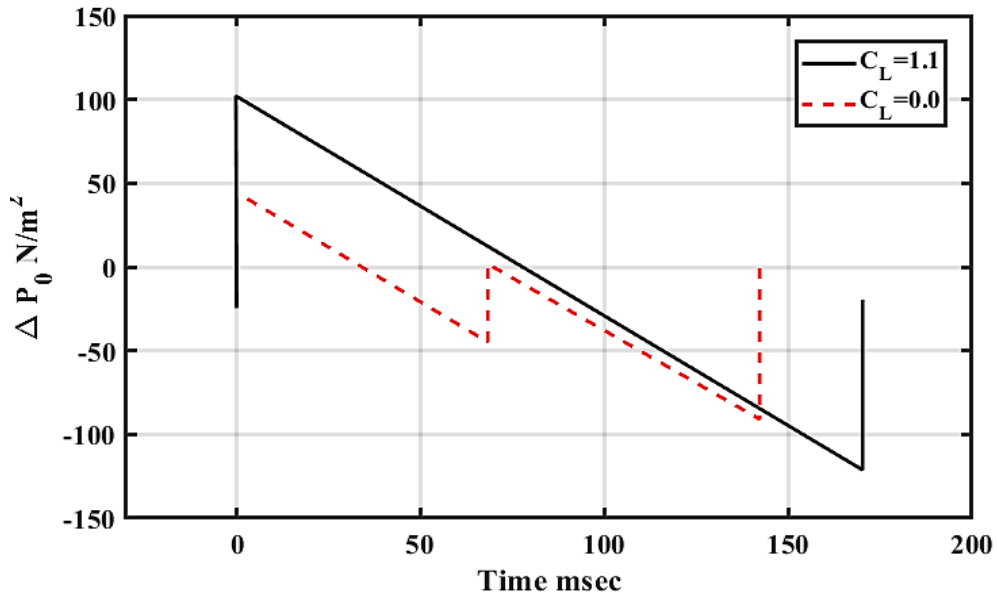


Figure 10: Effect of C_L on sonic boom signature as measured from ground

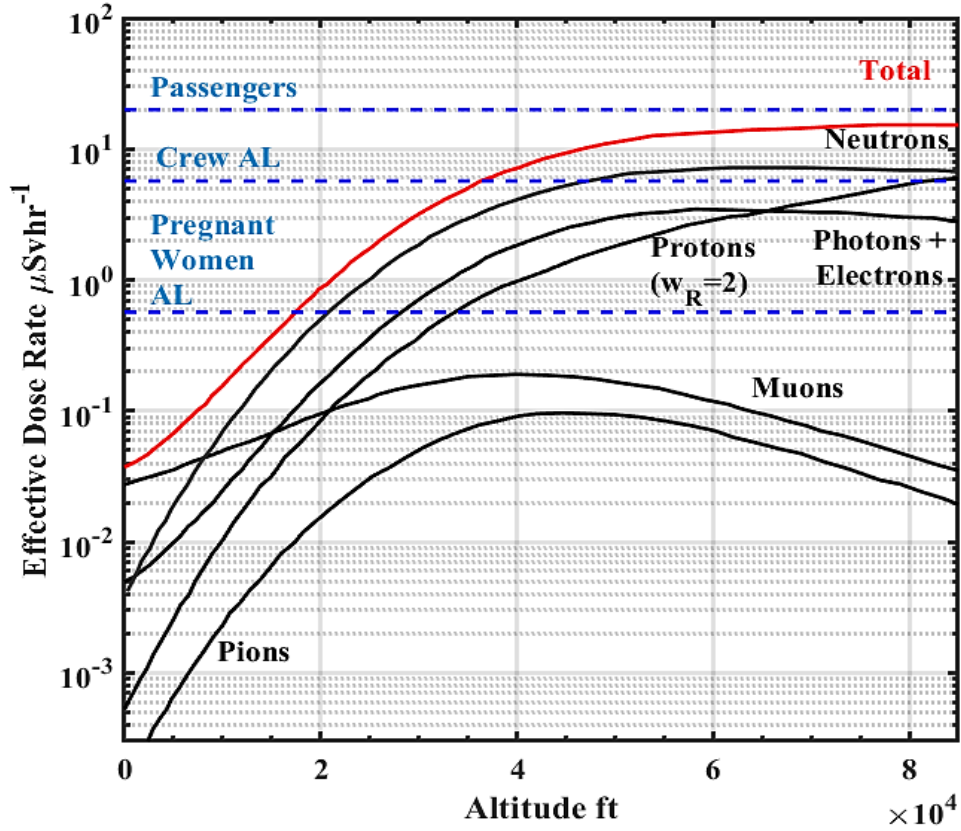


Figure 11: Effective dose rate of various radiation component vs altitude near the polar plateau (cutoff 5.08 GV) at solar minimum (June 1997)

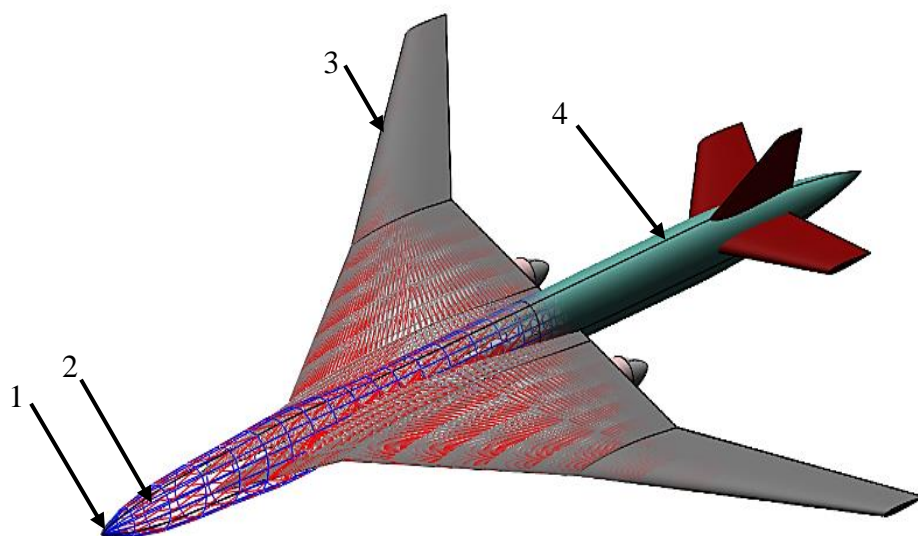
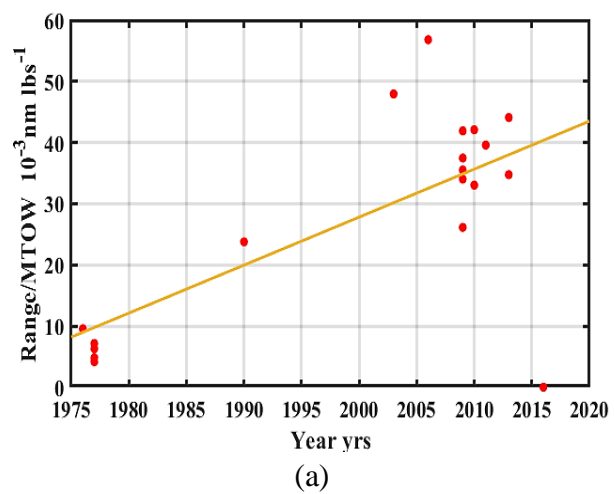


Figure 12: Critical components of an SCTA



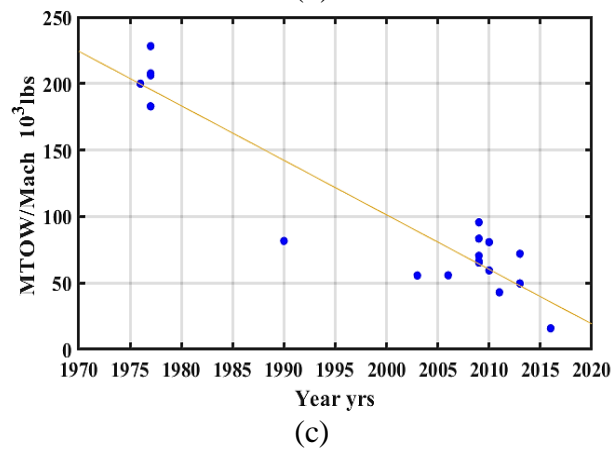
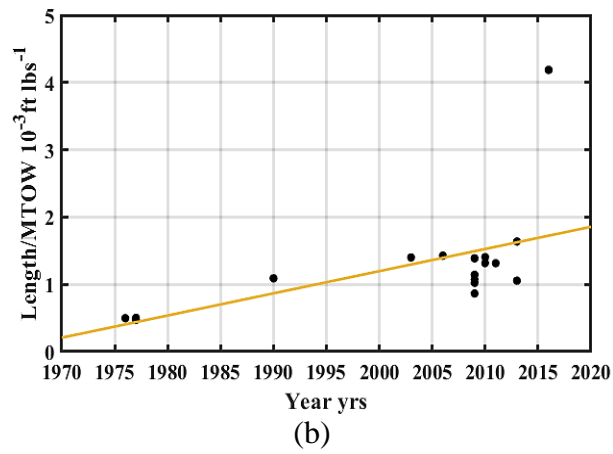


Figure 13: Trends of supersonic transport aircraft

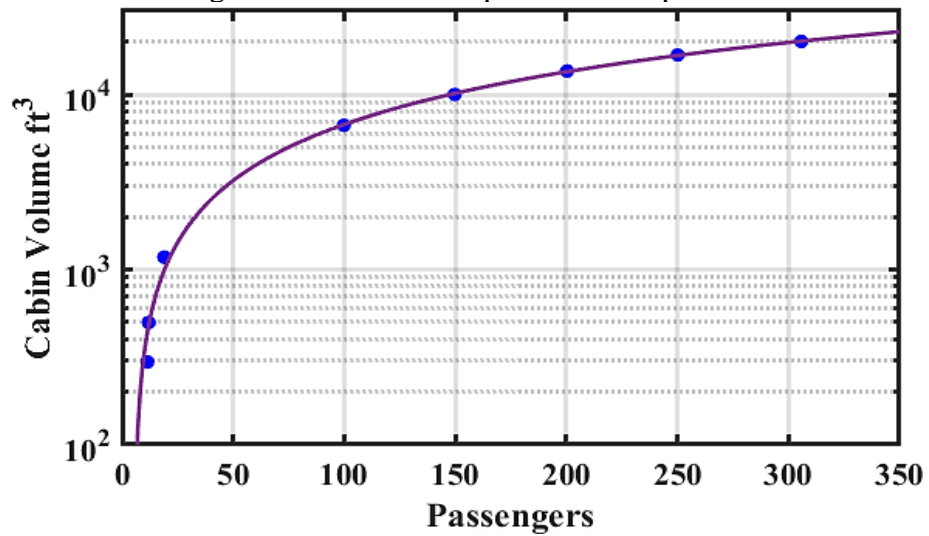


Figure 14: Number of passengers vs cabin volume

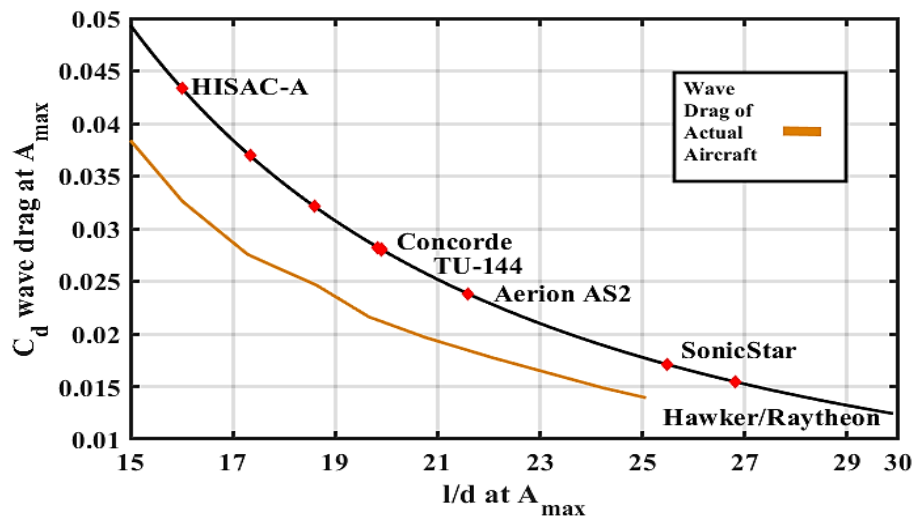


Figure 15: Supersonic wave drag for a Sear-Haack body with given constant maximum area

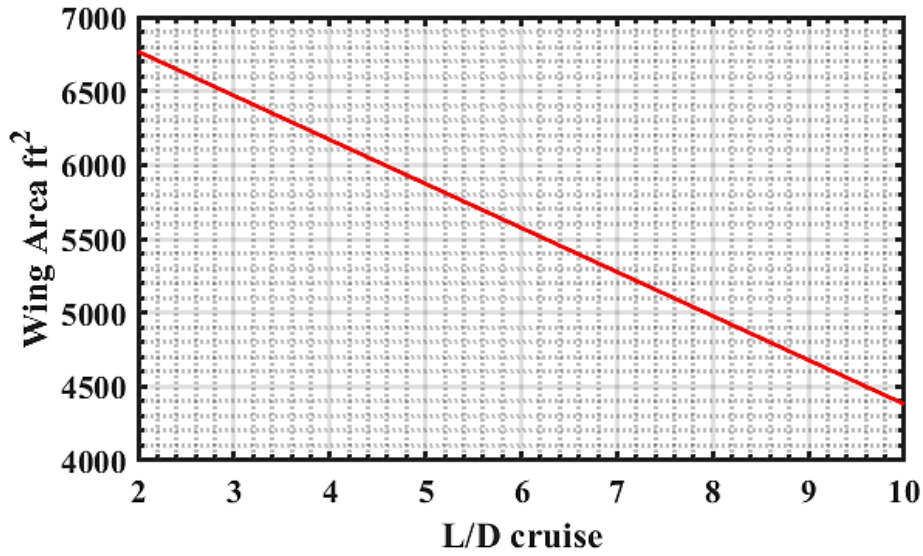


Figure 16: Estimation of swept back wing area based on L/D ratio

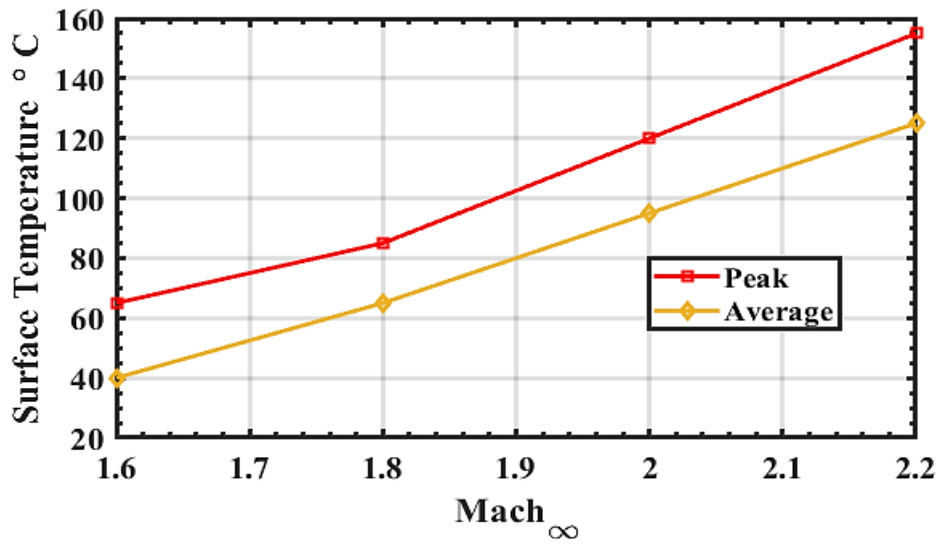
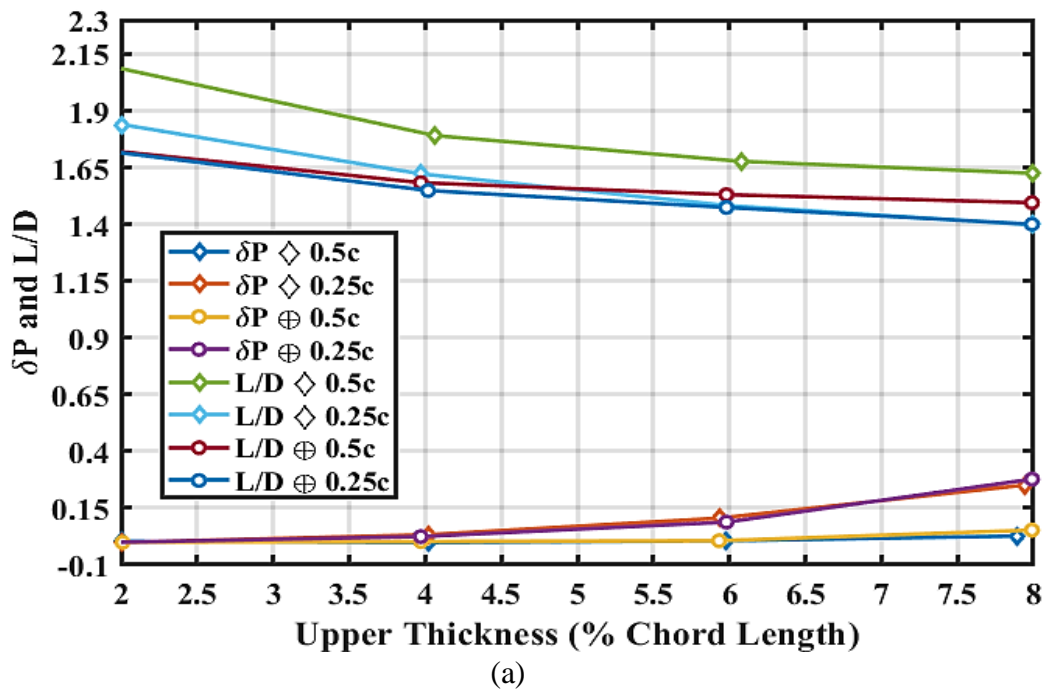


Figure 17: Surface temperature vs Mach number relationship



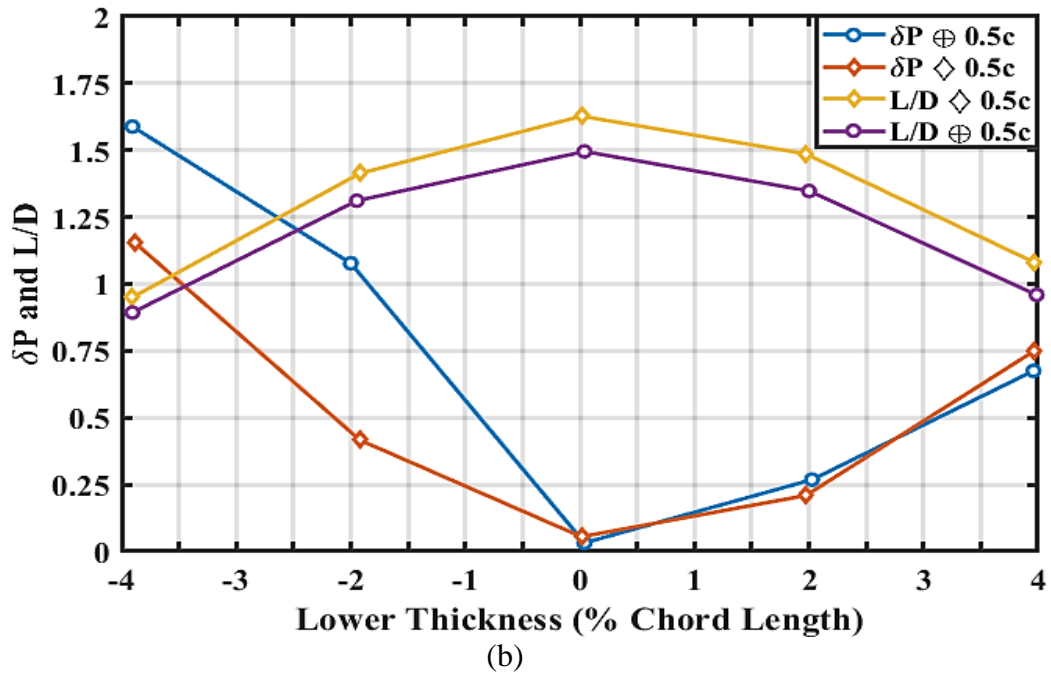


Figure 18: Supersonic performance of \diamond Diamond and \oplus convex airfoils for various camber thicknesses where $0.5c$ and $0.25c$ represents the chordwise distance where the maximum thickness occurs, with respect to the chord length c

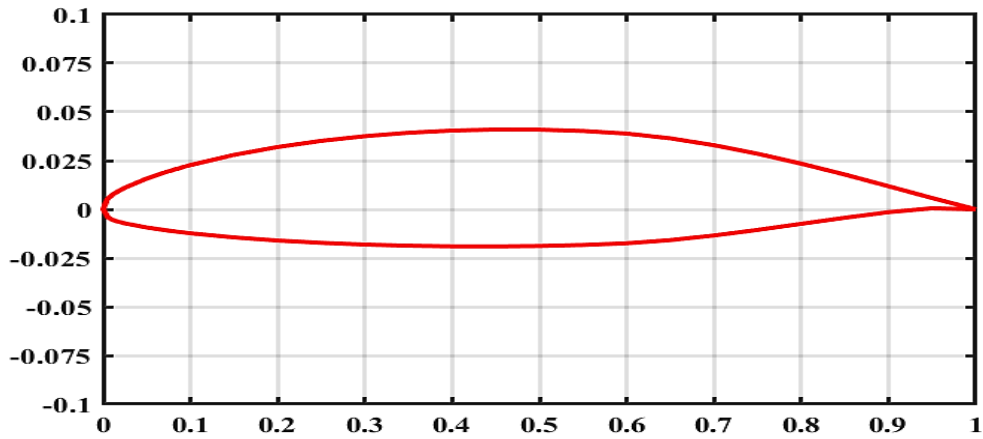
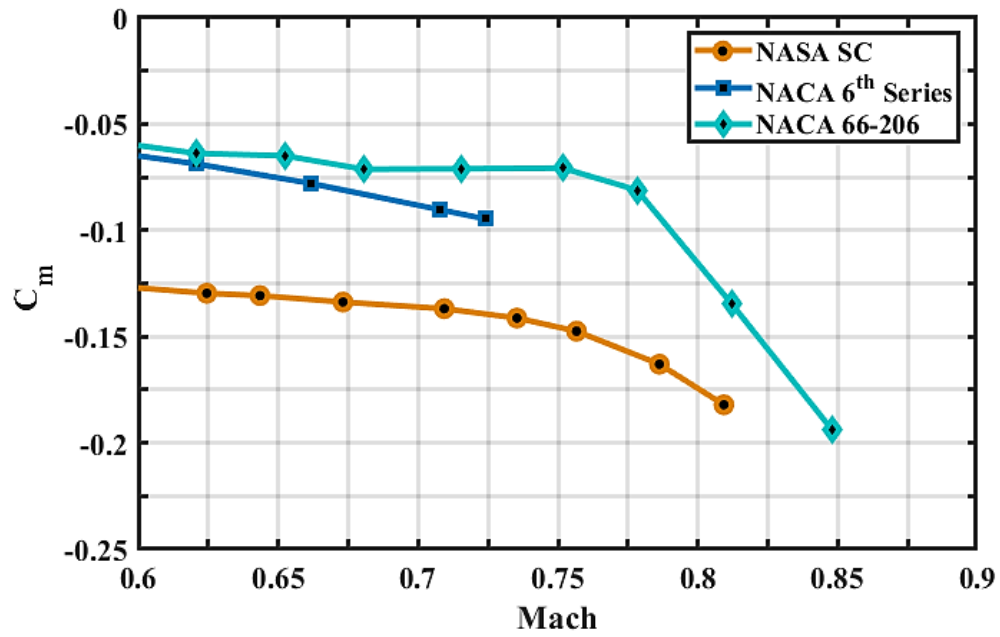
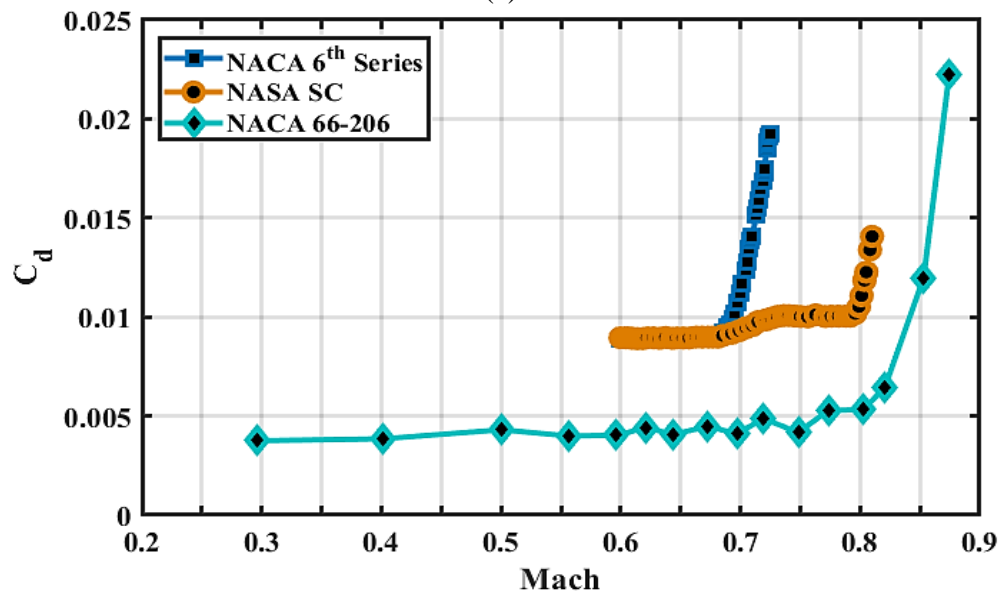


Figure 19: NACA 66-206

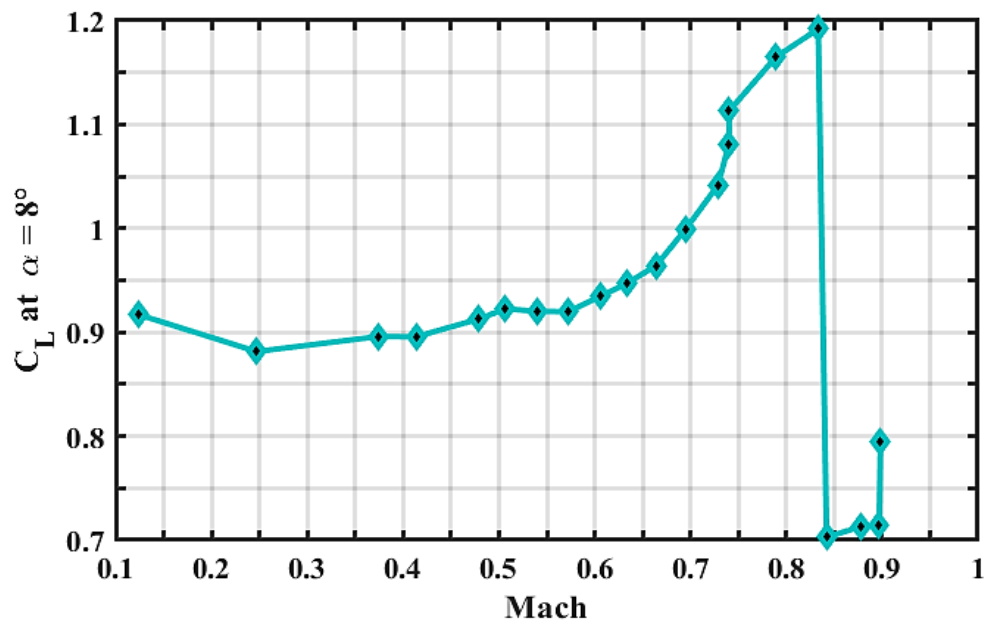


(a)

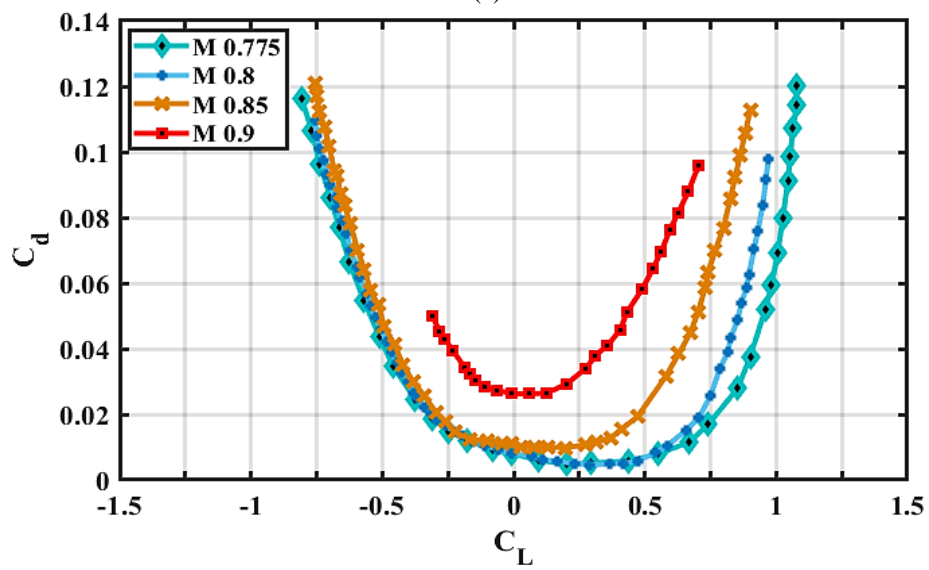


(b)

Figure 20: Pitching and drag performance comparison between different airfoils in the subsonic and transonic regime

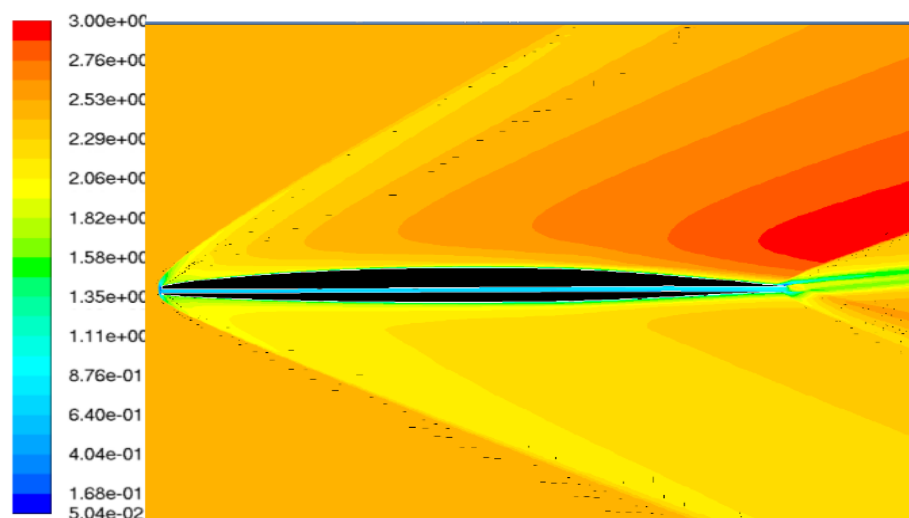


(a)



(b)

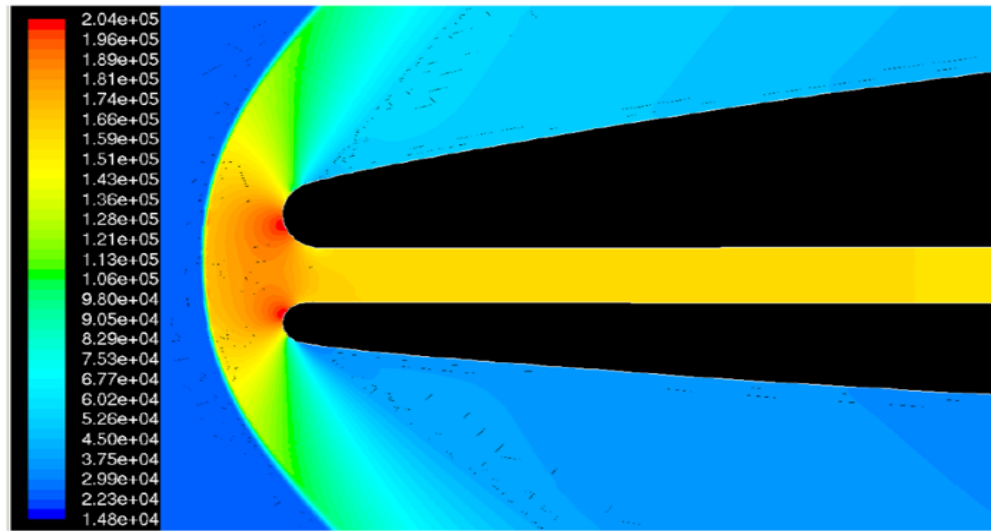
Figure 21: Lift and drag-polar of NACA 66-206



(a)



(b)



(c)

Figure 22: Influence of a supersonic channel. (a), (b) shows Mach lines whereas (c) shows pressure contours. The simulations were done an α of 6° and altitude of 35,000 ft

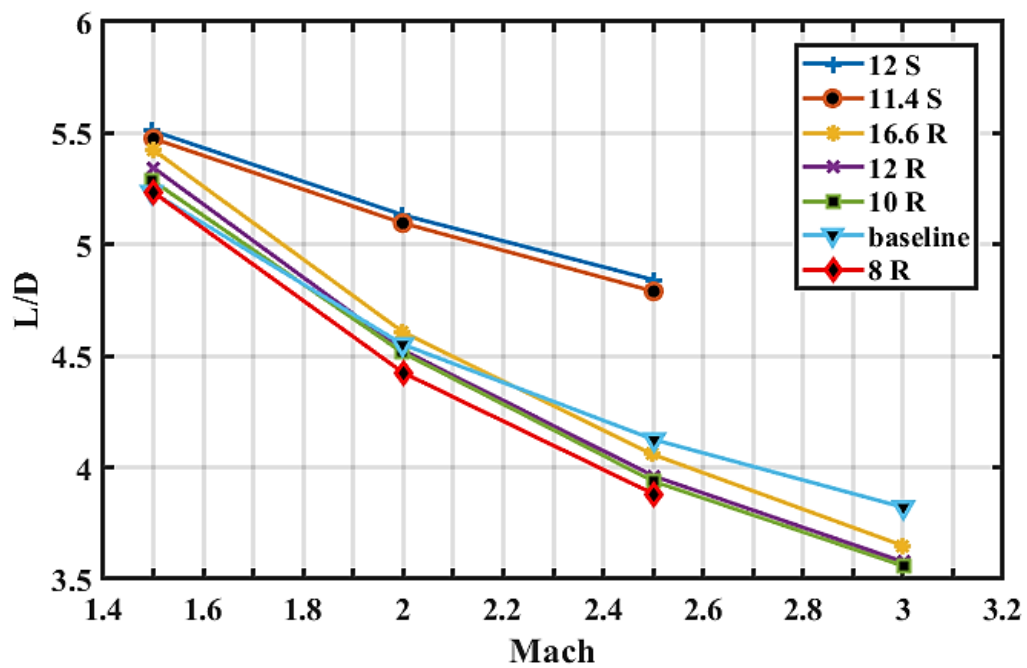
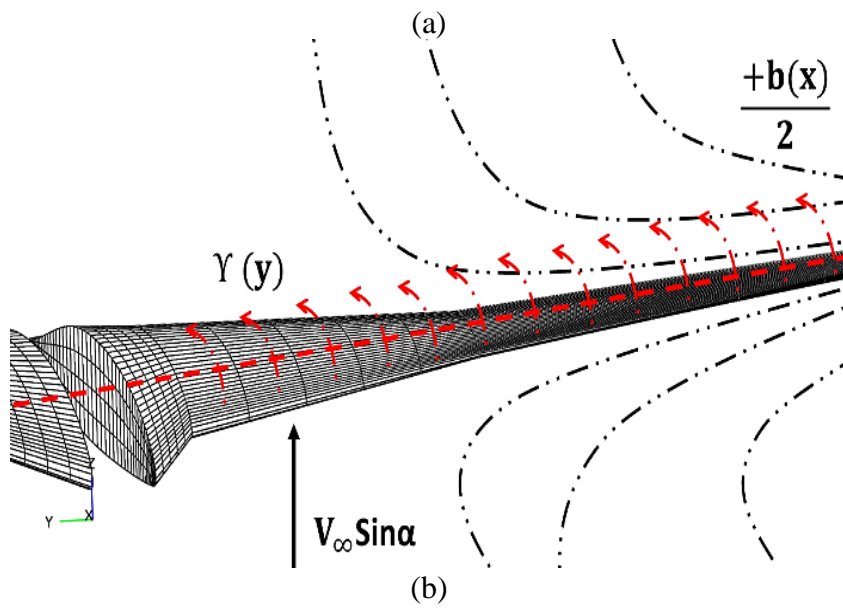
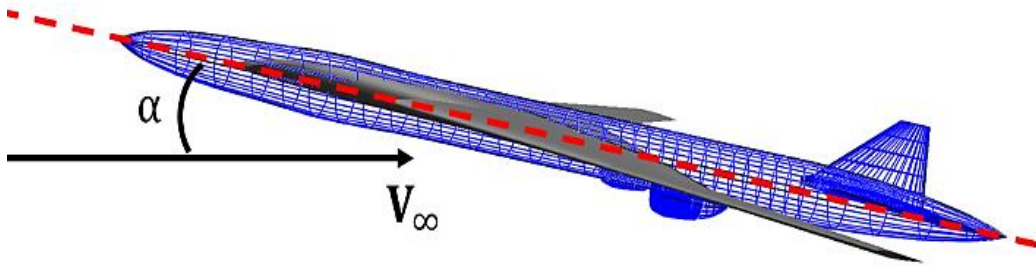


Figure 23: Effects of channel height and its edge sharpness on the lift-to-drag ratio of the airfoil. S and R represents sharpened and rounded edges respectively. The simulations were done an α of 6° and altitude of 35,000 ft



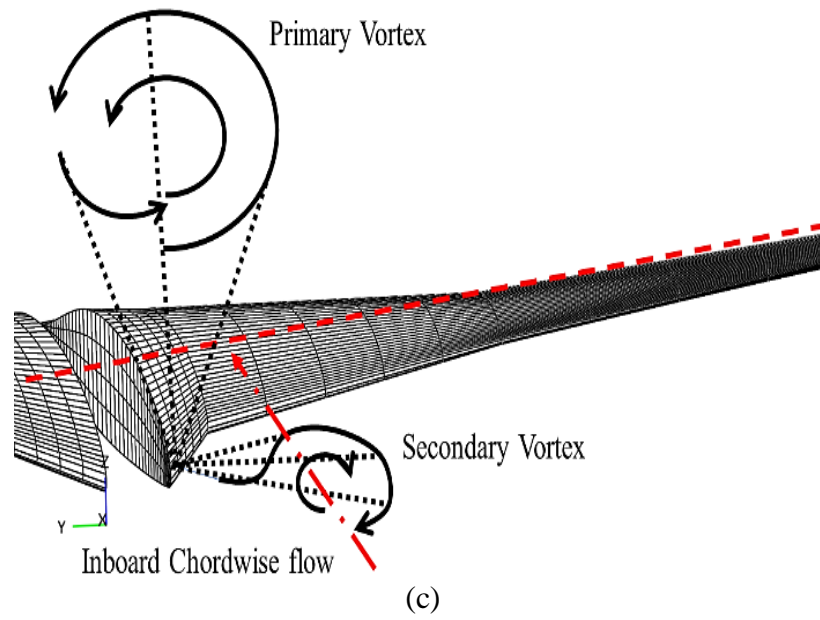


Figure 24: (a), (b) Potential flow 2D discretization, (c) Houghton and Carpenter vortex correction for high angles of attack.

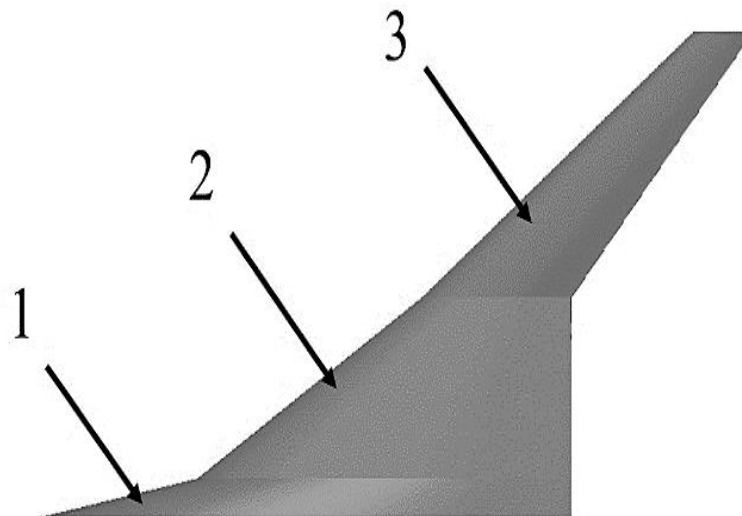


Figure 25: Wing section identification

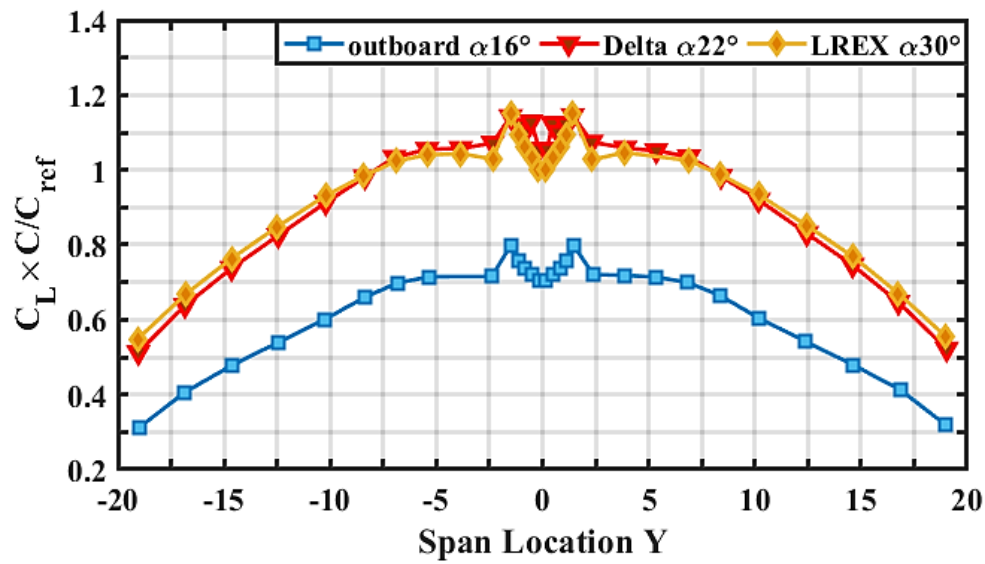
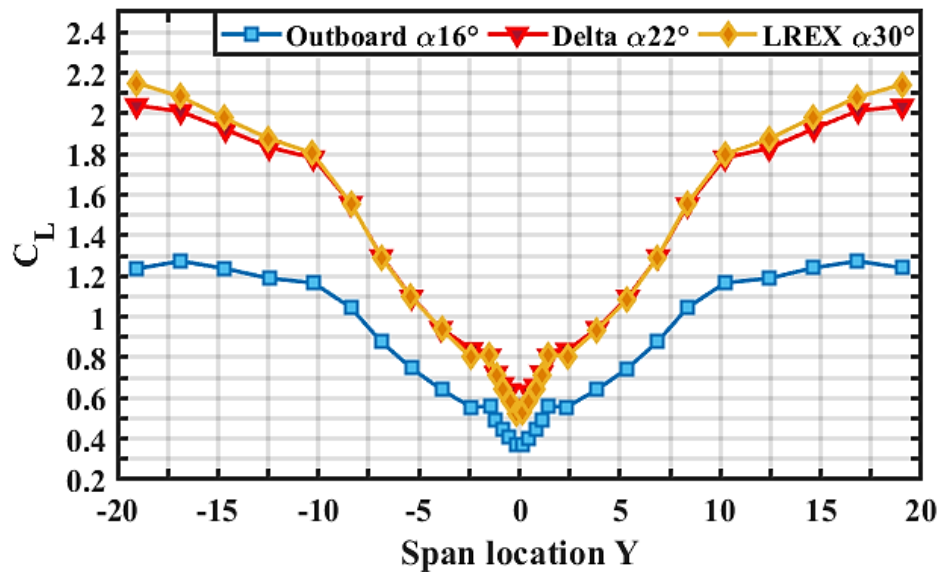


Figure 26: Normalized wing loading at $\alpha_\infty = 12^\circ$ and $M = 0.3$



(a)

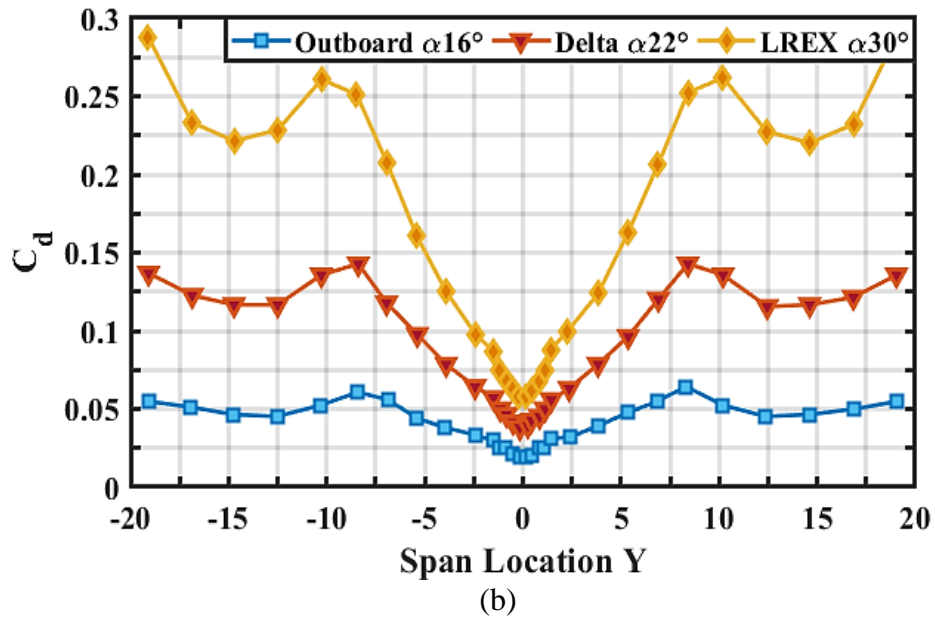


Figure 27: Local lift and drag distribution at $\alpha_\infty = 12^\circ$ and $M = 0.3$

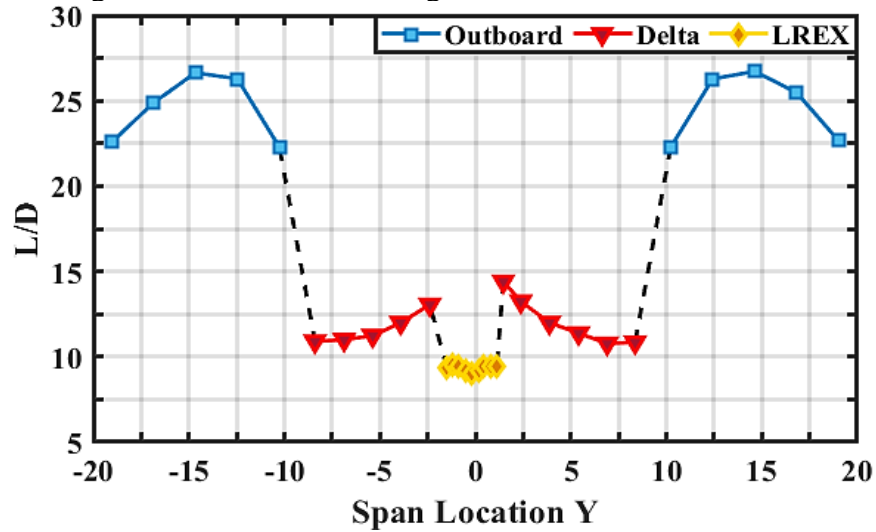


Figure 28: Local lift to drag ratio distribution at $\alpha_\infty = 12^\circ$ and $M = 0.3$

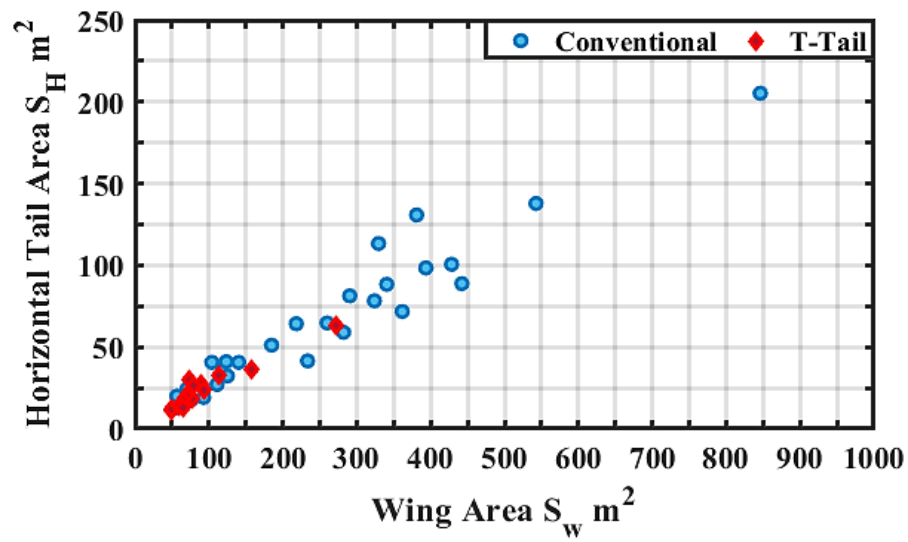


Figure 29: Correlation between horizontal tail and wing

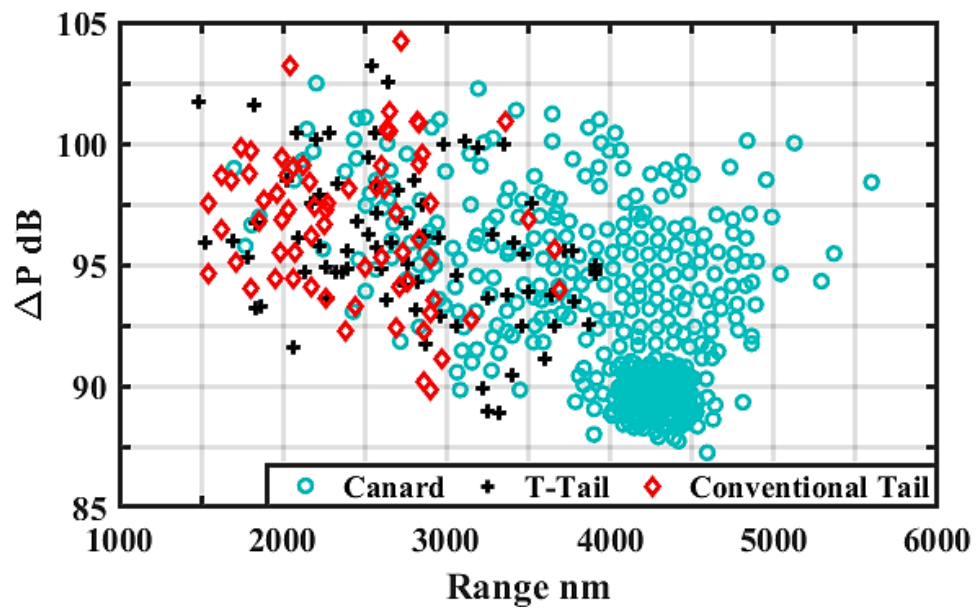


Figure 30: Sonic boom performance for different tail configuration

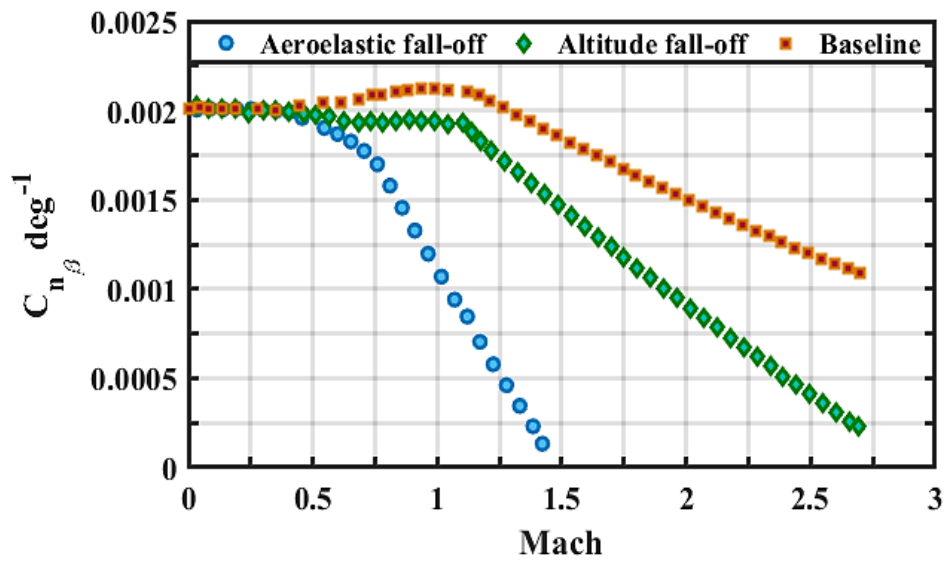


Figure 31: Directional stability fall-off with increase in Mach number

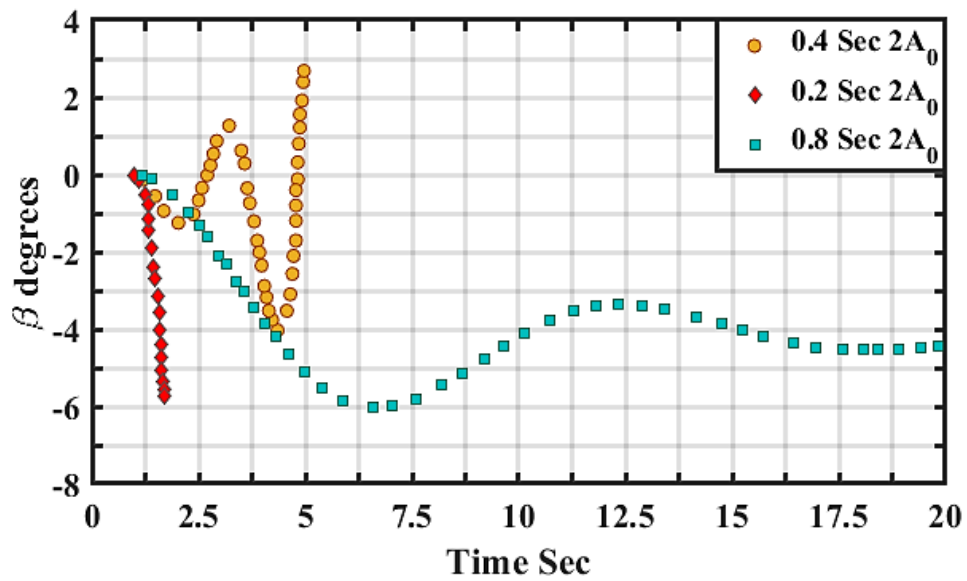
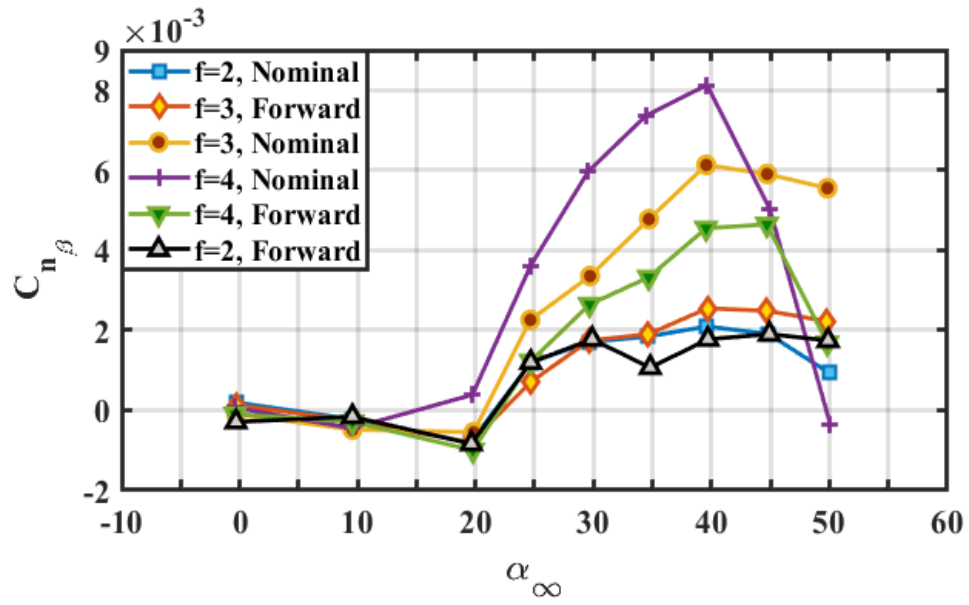
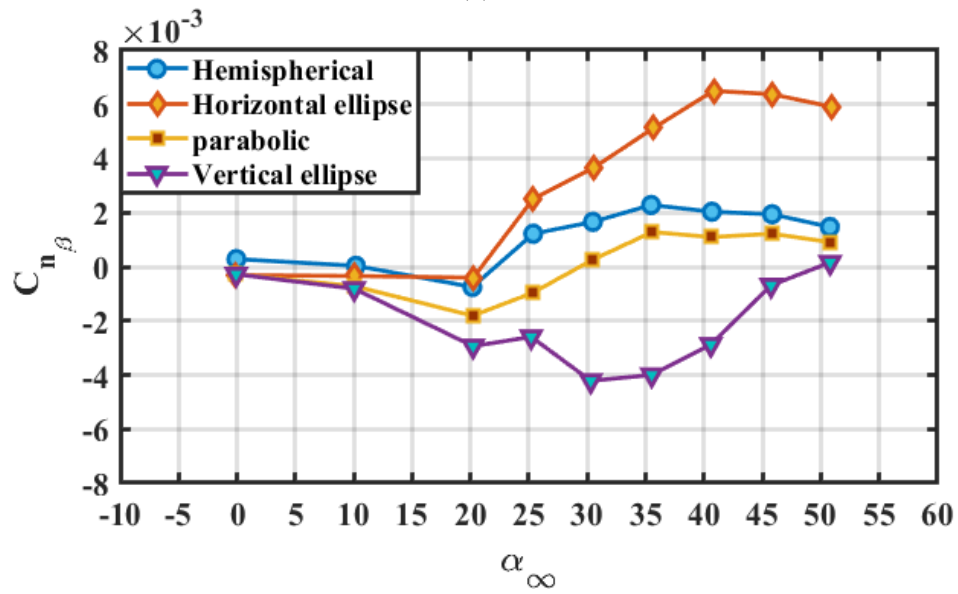


Figure 32: System response to different doubling side slip angle perturbation functions

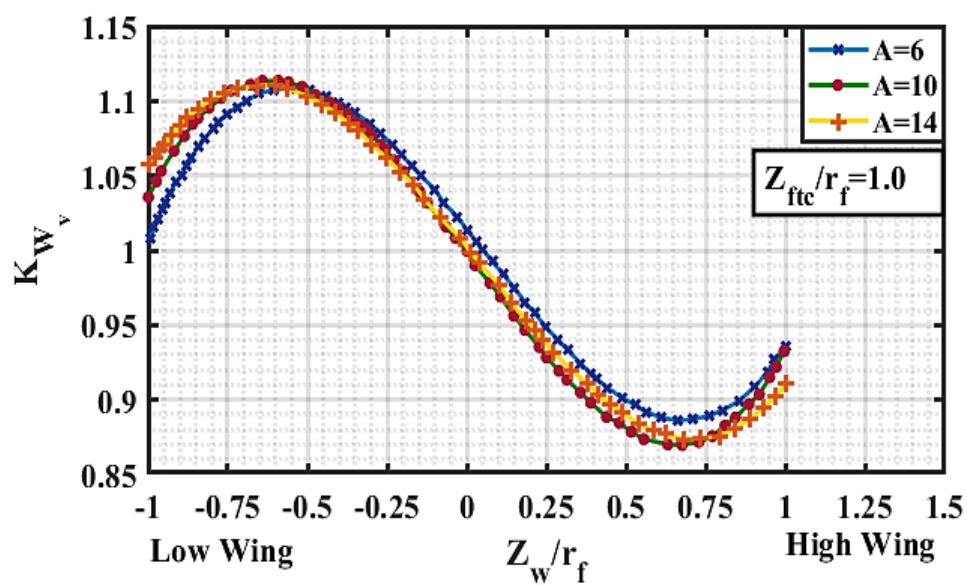


(a)

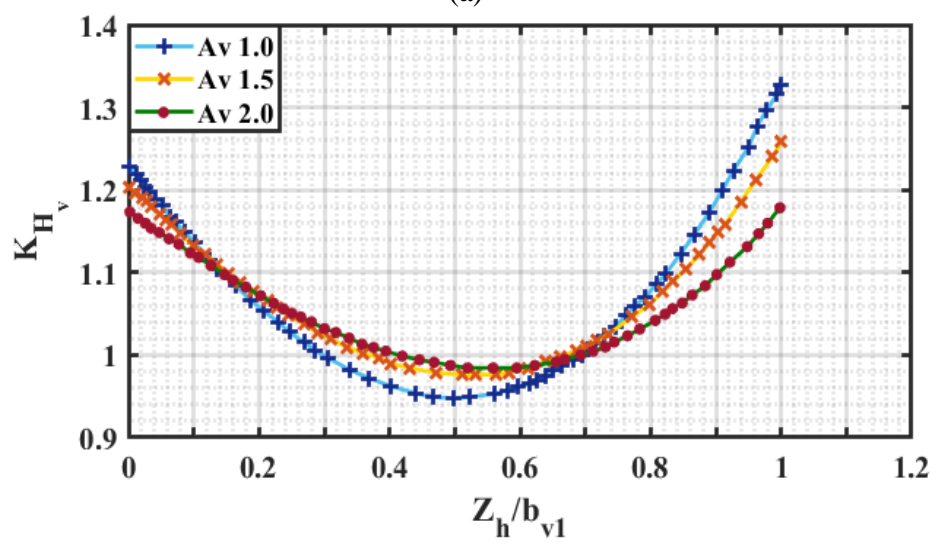


(b)

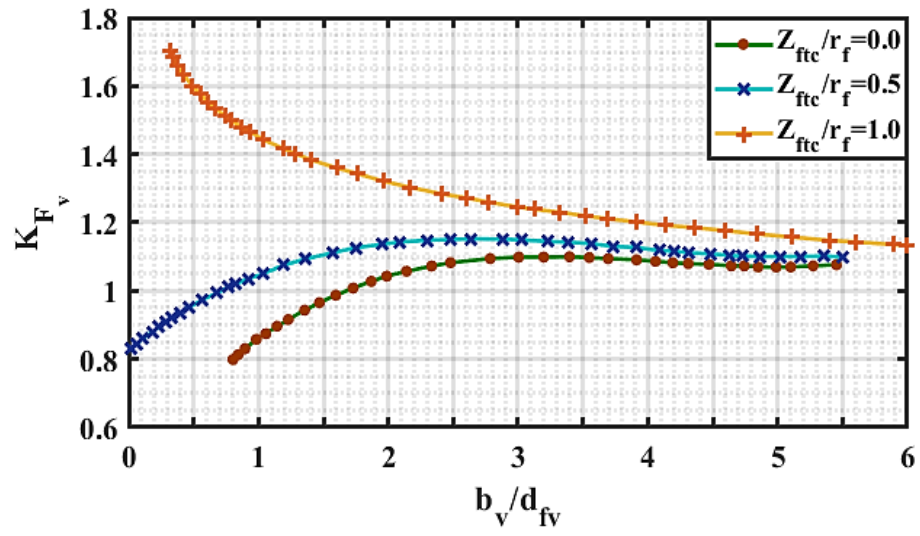
Figure 33: (a) Effect of fuselage cross-sectional shape on directional stability (fineness ratio = 3; nominal wing position), (b) Effect of fineness ratio and wing proximity on directional stability, horizontal ellipse forebody



(a)



(b)



(c)

Figure 34: (a) Effects of wing, (b) Effect of Horizontal tail (High Wing), and (c) fuselage on vertical tail.

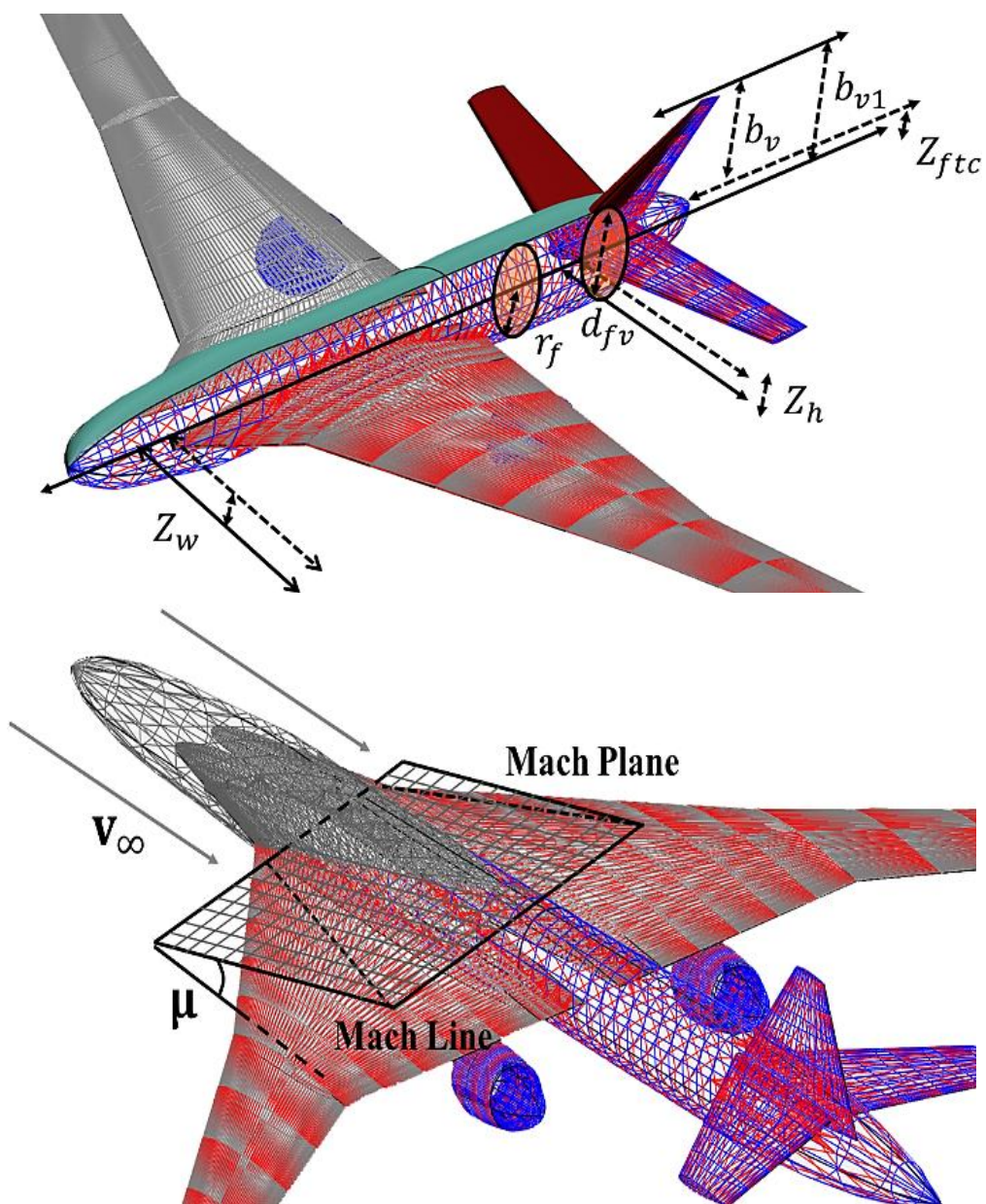


Figure 35: Elaboration of Figure 36: Mach Planes discretization parameters

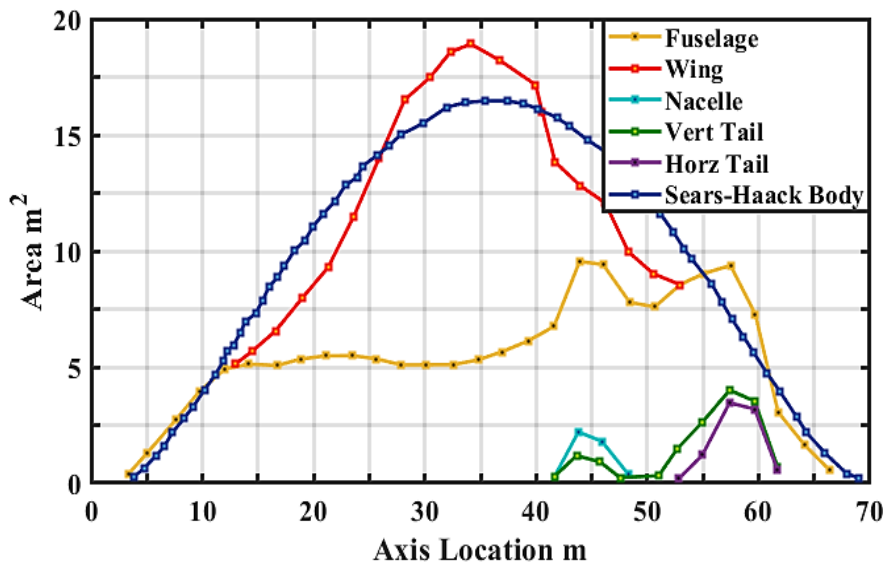


Figure 37: Supersonic area ruling

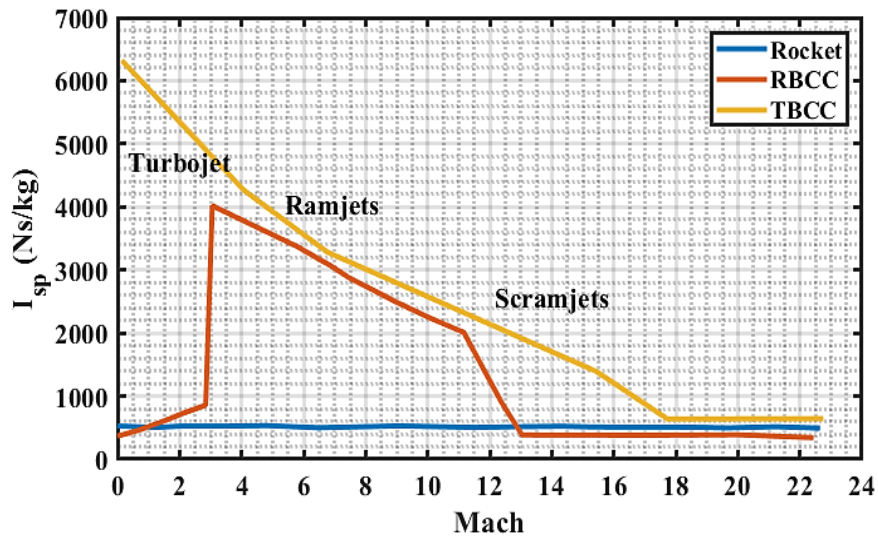


Figure 38: Specific thrust impulse of different propulsion drives

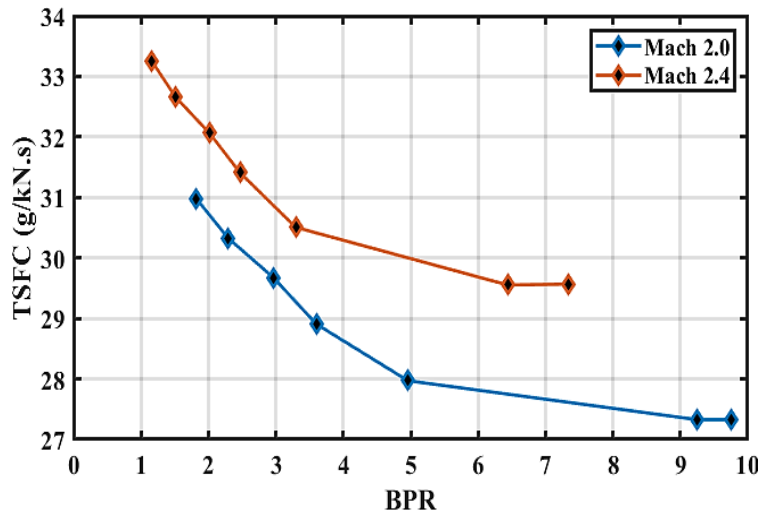


Figure 39: effect on TSFC for various bypass ratio at different cruise Mach, each point optimized for maximum fan-efficiency. $\pi_c=15$, Turbine inlet total temperature =1940 K, h=60,000 ft.

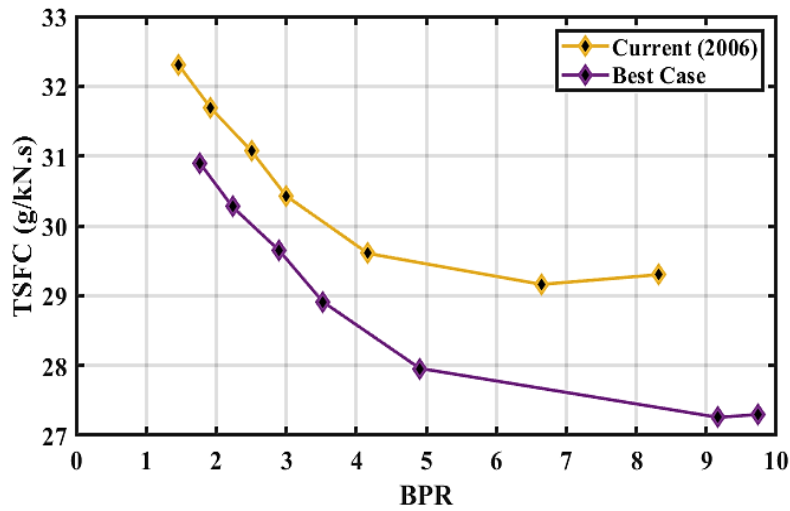


Figure 40: effect on TSFC for various bypass ratio for currently available and best case possible, each point optimized for maximum fan-efficiency, at M=2. $\pi_c=15$, Turbine inlet total temperature = 1940 K, h=60,000 ft.

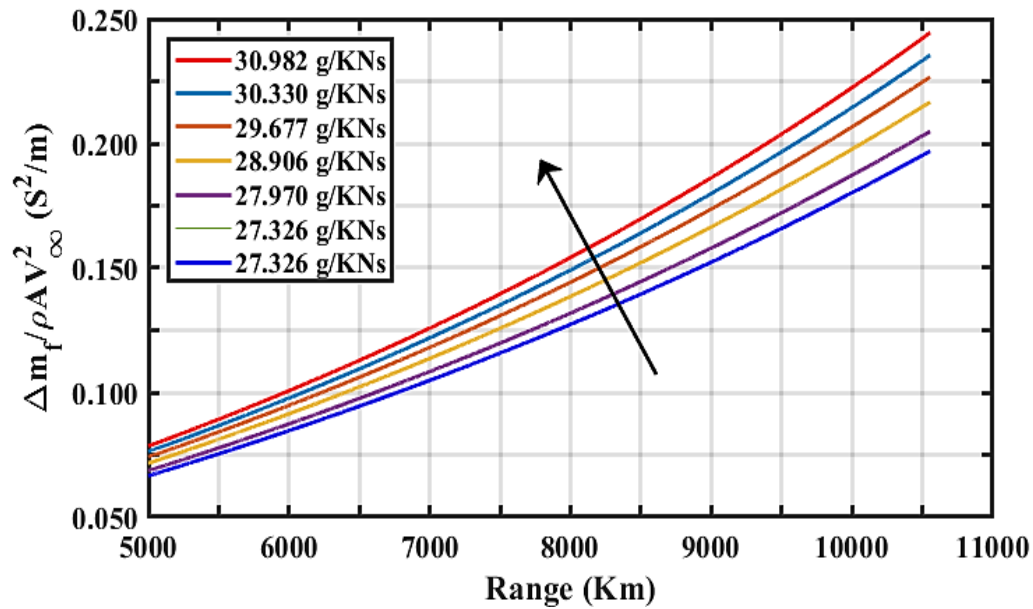


Figure 41: effect of TSFC on normalized fuel mass needed versus cruise range covered by the engine given $C_D = 0.011$ and $h=60,000$ ft.

List of Symbols & Abbreviations

MTOW	Maximum Take-off Weight	W_a	Weight of the component due to material 'a'
GTOW	Gross Take-off Weight	W_e	Empty weight of the aircraft
M	Median	H	Altitude
σ	Standard Deviation	P_0	Ambient pressure at ground
$ \Sigma $	Cumulative of absolute values	P_a	Ambient pressure at altitude
A_i	Net surface area of i^{th} component	ΔP_0	Measured pressure rise across shock wave at ground
C_i	Cost index value of i^{th} component	k_r	Ground reflection factor
k_i	Cost of the material per m^2 of i^{th} component in chosen currency unit	k_b	Body shape factor
S_{eq}	Equivalent area	d	Diameter of circle equivalent in area to the airplane cross-sectional area
ρ	Local air density	l	Length of aircraft
ρ_∞	Free stream density	L_{rf}	Length of rear end of fuselage
ρ_a	Density of material 'a'	b	Wing span of the aircraft
v	Local slip stream velocity	h	Height of the aircraft
v_∞	Free stream velocity	H_f	Height of fuselage
M	Local Mach number	S	Wing span area
M_∞	Free stream Mach number	S_h	Horizontal tail area
M_β	Vertical tail side slip Mach number	S_{elv}	Elevator area
W	Instantaneous gross weight	V_{cb}	Cabin volume

R	Lateral distance from the flight track on ground	c_p, c_{dp}	Lift and drag coefficients for potential flow
BPR_{rel}	Relative takeoff by-pass ratio	c_{lv}, c_{dv}	Lift and drag coefficients for vortex flow correction
TTO_{rel}	Relative takeoff turbine rotor temperature	c_{d0H}	Horizontal tail zero-lift drag coefficient
OPR	Overall pressure ratio		
$TR_{TO re}$	Relative takeoff thrust throttle ratio	c_{lH}	Horizontal tail lift coefficient
W	Relative wing loading	c_{lw}	Wing co-efficient of lift
$/S_{rel}$		c_{mw}	Wing co-efficient of pitch moment
WL	Absolute wing loading	Λ	Sweep angle
ΔR_{rel}	Relative change in range	$\Lambda_{v.c/2}$	Vertical tail sweep at C/2
\bar{R}	Absolute range	AR	Aspect ratio
dE_{max}	Change in jet noise level	AR_H	Horizontal tail aspect ratio
D_{pv}	Corrected cruise NOx emission	AR_v	Vertical tail aspect ratio
dT_{ns}	Change in near surface temperature	C_r	Root chord length
$EINO_{xcl}$	Average cruise NOx emission index	\bar{C}	Mean chord length
W_{fcr}	Total cruise fuel consumption	\bar{C}_w	Wing mean aerodynamic chord
σ_{va}	Yield strength of material 'a'	λ	Taper ratio
E_a	Young's modulus of material 'a'	λ_H	Horizontal tail taper ratio
LDR	L/D ratio	$\alpha_{L=0}$	Zero lift angle of attack
Δt	Number of years	α_i	Induced angle of attack
n_b	Number of passengers	ζ_{SCC}	Supersonic channel correction factor
D_{wave}	Wave drag of the aircraft	η_H	Horizontal tail dynamic pressure ratio
D_H	Drag of horizontal tail		
D_{Hind}	Induced horizontal tail drag	v_{eH}	Horizontal tail volume coefficient
D_{Hi}	Horizontal tail induced drag parameter	x_{cg}	Aircraft's center of gravity
$C_{D_{wv}}$	Co-efficient of wave drag	x_{ac}	Aerodynamic center
s	Slenderness ratio	β	Side-slip angle
α	Local angle of attack	$c_{n\beta}$	Directional stability derivative coefficient
α_∞	Free stream angle of attack		
α_t	Horizontal tail strike angle	$c_{l\beta_v}$	Vertical tail lift slope
φ	Velocity potential	$c_{n\beta_v}$	Vertical tail directional stability derivative coefficient
\emptyset	Efficiency factor of aircraft's polar	ε	Compressibility factor
p_t	Total pressure	k	Section lift slope factor
p	Static pressure	K_{Fv}	Fuselage-vertical tail interaction correction factor
C_{dp}	The drag of a flat plate perpendicular to a free stream	K_{Wv}	Wing-vertical tail interaction correction factor
c_l	Co-efficient of lift	K_{Hv}	Horizontal tail-vertical tail interaction correction factor
c_d	Co-efficient of drag		
c_m	Co-efficient of pitching moment		